JOURNAL OF SPACECRAFT AND ROCKETS
Vol. 36, No. 3, May–June 1999

Analysis of Galileo Probe Heatshield Ablation and Temperature Data

F. S. Milos,* Y.-K. Chen,† and T. H. Squire‡
NASA Ames Research Center, Moffett Field, California 94035-1000
and
R. A. Brewer§
Lockheed Martin Missiles and Space Company, King of Prussia, Pennsylvania 19406

The Galileo Probe deceleration module contained instrumentation to measure heatshield ablation and temperatures during its hypersonic entry into the atmosphere of Jupiter. The ablation data reduction and analysis were reported previously; therefore, only a brief review is provided. One-dimensional transient analyses of the heatshield ablation, pyrolysis, and heat conduction were performed at the thermometer locations. These calculations were coupled with an axisymmetric heat conduction model to predict the thermometer temperature response. Near the end of the frustum, the temperature and recession data are very consistent. The measured recession is 3.63 ± 0.15 cm, and the estimated peak heat flux and heat load are 13.4 ± 0.5 kW/cm^2 and 161 ± 6 kJ/cm^2, respectively. At the aft cover, the material response analyses do not match the low magnitude and slope of the temperature data, which seem to indicate that heat conduction into the heatshield was lower than expected.

Nomenclature

c	= curve-fit constant, s^{-1}
c_p	= heat capacity, J/kg-K
h	= enthalpy, J/kg
k	= thermal conductivity, W/m-K
M	= forebody heatshield mass, kg
$\dot{m}$	= surface mass flux, kg/cm^2-s
Q^*	= heat of ablation, J/kg
q_{cond}	= conduction heat flux, W/cm^2
q_{net}	= heat flux to surface, W/cm^2
S/R_N	= dimensionless streamlength from nose
s	= recession, cm
s_m	= total recession, cm
$\dot{s}$	= recession rate, cm/s
T	= temperature, K
T_{abl}	= ablation temperature, K
t	= time after entry, s
t_m	= time of maximum recession rate, s
ε	= emissivity
ρ	= density, kg/m^3
σ	= Stephan–Boltzmann constant, W/m^2-K^4

Subscripts

c	= char
g	= pyrolysis gas
i	= index for six S/R_N locations
s	= solid at surface
v	= virgin
w	= gas at surface

Presented as Paper 97-2480 at the AIAA 32nd Thermophysics Conference, Atlanta, GA, June 23–25, 1997; received Jan. 5, 1998; revision received Aug. 15, 1998; accepted for publication March 12, 1999.

*Aerospace Engineer, Thermal Protection Materials and Systems Branch. Senior Member AIAA.
†Aerospace Engineer, Thermal Protection Materials and Systems Branch.
‡Senior Research Scientist, ELORET Thermosciences Institute.
§Project Technologist, Aerothermophysics Unit.

Introduction

THE Galileo Probe deceleration module encountered the most severe heating environment ever experienced by a planetary entry probe when it entered the atmosphere of Jupiter at a relative velocity 47.4 km/s on Dec. 7, 1995. As the probe decelerated from Mach 50, the forebody heatshield had to survive a peak heating rate and a heat load on the order of 30 kW/cm^2 and 300 kJ/cm^2, respectively, for the nominal entry conditions.[1–4] The heatshield also was required to maintain the structural bondline temperature below 644 K and the structure below 589 K prior to parachute deployment, which released the heatshield from the descent module containing the primary scientific instruments.[1,3]

Figure 1 shows a cross section of the deceleration module.[3–6] The forebody exterior shape was an axisymmetric sphere–cone with 22.2-cm nose radius and 44.86-deg half-angle. The aft exterior shape was an annulus section connecting to a spherical aft cover with outer radius of 62.1 cm. The nosecap was chopped-molded carbon phenolic, the frustum was tape-wrapped carbon phenolic, and the aft heatshield was phenolic nylon. The forebody heatshield thickness decreased from 14.6 cm at the centerline to a minimum of 5.1 cm at the front of the frustum, then increased to 5.4 cm at the rear of the frustum. The thickness of the aft cover decreased from 1.04 cm on the centerline to 0.89 cm near the annulus section. These thickness distributions provided about a 50% safety margin[3] against conservative predictions of heatshield recession for the nominal axisymmetric entry at −8.6 deg into a nominal atmosphere containing 89% H_2 and 11% He. This margin was believed to be adequate for probable survival of the probe under a worst-case scenario of steep entry at −10.0 deg into a cool–heavy atmosphere containing 25% He. As summarized in Table 1, the actual entry[7] was slightly shallow (−8.4 deg), and the atmosphere[8,9] was somewhat heavy (13.6% He). The probe survived this entry, but the distribution of mass loss differed from predictions.[10]

As shown in Fig. 2, the deceleration module contained 10 recession sensors embedded in the forebody heatshield and four resistance thermometers bonded to the inside of the structure.[11] The measurements obtained from these sensors and thermometers are the only data available for assessment of the entry environment and heatshield performance of an outer planet entry probe. A detailed description of the recession sensors, reduction of the recession data, reconstruction of the heatshield shape history, and comparisons with preflight predictions were presented in Ref. 10. For completeness, that work is briefly reviewed here; however, the primary purpose of the present work is performance of heatshield thermal response

Table 1 Galileo Probe entry conditions

Condition	Nominal (range)	Actual
Entry velocity, km/s	47.8	47.4
Entry angle, deg	−8.6(±1.4)	−8.4 ± 0.1
Attack angle, deg	0 (0–6)	<7.0
Mole percent He	11 (0–25)	13.6 ± 0.3
Molecular weight	2.22 (2.0–2.5)	2.35[a]
Rotation rate, rpm	10.5 ± 0.5	10.5

[a]Including heavy trace species NH_3 and CH_4 (Ref. 9).

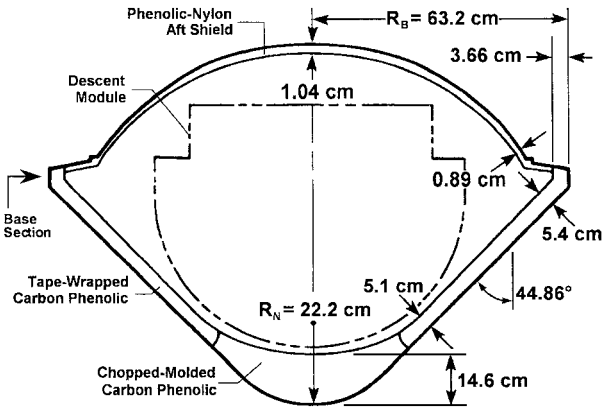

Fig. 1 Cross section of Galileo Probe deceleration module.

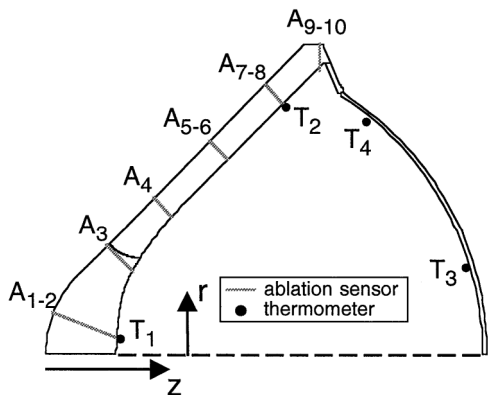

Fig. 2 Locations of 10 ablation sensors (A_1–A_{10}) in heatshield and four resistance thermometers (T_1–T_4) inside structure; sensors are not coplanar.

calculations to check the self-consistency of the ablation and temperature data and to estimate the surface heating at the thermometer locations.

Review of Heatshield Ablation Experiment

In the forebody heatshield 10 analog resistance ablation detector (ARAD) sensors[12] were installed at six S/R_N locations shown in Fig. 2 and listed in Table 2.[11,13] The sensors were passive resistive elements designed to ablate concurrently with the heatshield and were connected to precision constant-current sources to provide a voltage proportional to the sensor length. The nosecap sensors (A_1–A_3) and frustum sensors (A_4–A_{10}) were on separate circuits with independent current sources. The current sources and sensor resistances were calibrated to provide a nominal measurement uncertainty of ±0.091 cm for recession.[3] During probe entry into the Jovian atmosphere, voltage data from each ARAD were taken at an average sampling interval of 0.57 s (Ref. 14). The data passed through analog-to-digital(A/D) conversion and were stored as 8-bit binary numbers (0–255 in decimal count) in recycling memory.[15] The stored data spanned the ablative portion of the trajectory and contained 84 measurements from each ARAD.

Data acquisition could be terminated by several conditional and unconditional events based on the status of acceleration switches, resets, and timers. These events occurred between 74.8 and 85.1 s after the probe reached an altitude 450 km above the 1-bar pressure level,[7] which is defined herein as time zero for entry. Because of the unknown effects of acceleration switch cross wiring in the probe, the absolute timing of the ablation data is not known with certainty. A timing reconstruction study suggests that data acquisition terminated at an unconditional event about 81 s after entry,[7,16] but comparison of the recession and trajectory data indicates that ARAD data acquisition probably ended at or near the first conditional event at 74.8 s. This earlier timing is used as a baseline in this work, but both timings are considered in the discussion of the results.

Table 2 ARAD locations and recession

ARAD	S/R_N (initial)	Final recession, cm	Heatshield thickness, cm	
			Initial	Final
1, 2	0.38	4.13 ± 0.25	14.15	10.02 ± 0.25
3	1.19	2.77 ± 0.25	7.40	4.63 ± 0.25
4	1.81	2.74 ± 0.15	5.17	2.43 ± 0.15
5, 6	2.55	3.13 ± 0.15	5.19	2.06 ± 0.15
7, 8	3.28	3.63 ± 0.15	5.30	1.67 ± 0.15
9, 10	3.96	2.58 ± 0.15	3.66[a]	1.08 ± 0.15[a]

[a]Relative to inside of heatshield base (cf. Fig. 2).

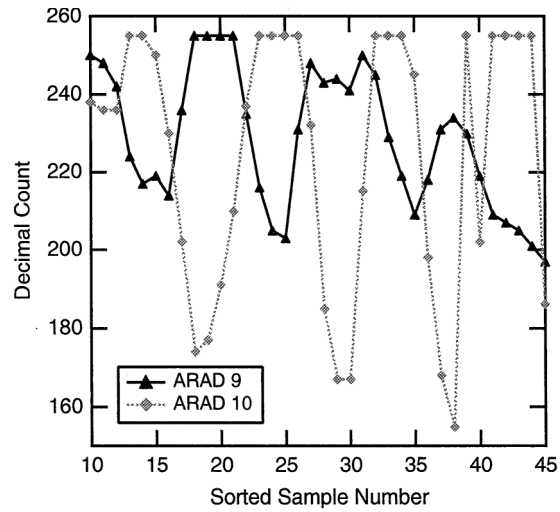

Fig. 3 Oscillations at 10.5 rpm in the ARAD data; one probe rotation is 10 samples or 5.7 s.

Sensor performance was compromised by an extraneous signal, which introduced oscillations into the first-half of the data. An example is given in Fig. 3 which shows several cycles of data oscillation at the probe rotation frequency (one full rotation every 5.71 s or 10 samples).[7] Some signal peaks were truncated at 255 counts by the A/D conversion. The count minima from ARAD 10 consistently lag similar minima from ARAD 9 by four to five samples (2.3–2.85 s), which is consistent with the 145.5-deg circumferential angle separation of these sensors and the spin direction of the probe. The data from the other sensors show similar oscillations and consistent phase lags between sensor pairs. The authors speculate that the probe surface acquired an electric charge or by some other mechanism interacted with ionized species in the high Mach number shock layer plasma, which caused an inadvertent voltage signal in the ARAD circuit. An alternative hypothesis is an interaction of the sensor circuit with the magnetic field of Jupiter.

The extraneous signal prevents establishment of a precise voltage baseline for the sensors at the start of the experiment. Based on the in-flight mission sequence test data,[17] a voltage offset of 0 to −5 counts is assumed for all ARAD measurements. Therefore, 2.5 counts are added to every ARAD data point prior to application of the calibration constant that converts voltage to sensor length.[15] The total recession uncertainty is assumed to be the sum of nominal measurement uncertainty plus a bias uncertainty of ±2.5 counts. This sum equals ±0.25 cm for nosecap ARADs 1–3 and ±0.15 cm for frustum ARADs 4–10. The uncertainty is larger for the nosecap

sensors because the nosecap circuit had a larger length per voltage count.

The ARAD data are plotted in Fig. 4 as recession vs time from entry, sorted by S/R_N location. Pegged data (255 counts) and a few other bad data points were excluded from the plots. The recession uncertainty is shown in the upper-left-hand corner of each plot. Also plotted on Fig. 4 are curve fits and bounding curves, which will be described later. The oscillations damp near 50 s, and the sensors provide nominal accuracy for the second-half of recession. The good agreement between the various sensor pairs confirms that ablation was axisymmetric to measurement accuracy. Axisymmetric final recession at the six S/R_N locations are listed in Table 2.

Histories of mass and shape-related quantities are needed for reconstruction of the trajectory and for determination of the atmospheric structure.[10,18] Because of the oscillations in the ablation data prior to 50 s, it is impossible to determine a precise history for the first half of the recession. Therefore, the approach taken in Ref. 10 was to define curve fits to the sorted recession data, which can be extrapolated backward in time to provide an estimated nominal history for the recession. Upper and lower bounds to the curve fits were also defined to provide estimates of the uncertainty in all derived quantities. The recession was fit with simple hyperbolic tangent functions s_i of the form

$$2s_i/s_{mi} = 1 + \tanh[c_i(t - t_{mi})] \tag{1}$$

which asymptotically approach the correct final recession values s_{mi} and which have a maximum slope at time t_{mi} when $s_i = s_{mi}/2$. The recession history is not necessarily a symmetrical function of $t - t_{mi}$, but the data quality is inadequate to justify the use of more sophisticated (skewed) fitting functions that contain additional constants. Upper and lower bound functions are defined by shifting the curve fits upward by the measurement uncertainty Δs_i and backward by a time uncertainty Δt. The lower-bound function was extrapolated linearly backward in time to provide a more conservative result. The curve-fit parameters are listed in Table 3. The general trend is for the peak recession rate to occur sooner on the frustum than on the nosecap, as indicated by the decreasing values of t_{mi} in Table 3. This trend may be a consequence of turbulence, which affects both convective and radiative heating, being more severe on the frustum than on the nosecap. The base recession, however, lags the frustum recession by more than 2 s. Curve-fit 3 to ARAD 4 is speculative but based on the curve fits obtained for the other sensors.

The nominal curve fits and the upper and lower bounding functions are presented with the recession data in Fig. 4. A time uncertainty $\Delta t = 0.5$ s provided reasonable bounds for the data. The fitting functions are within the nominal uncertainty of the data after the extraneous oscillations damp between 45 and 50 s. The bounding functions indicate that recession uncertainty reaches a maximum between 45 and 50 s, then decreases to the nominal measurement uncertainty for $t > 60$ s. The uncertainty is highest for the first two locations because ARADs 1–3 are the most sensitive to the voltage bias.

The curve fits provide time histories for six points on the forebody heatshield surface. A heatshield shape can be reconstructed by defining a series of three conical frusta, which connect the four frustum points, defining a spherical nose that passes through the first point and is tangent to the extension of the first frustum section, extending the last frustum section toward the base, and truncating the geometry at a base radius given by the last ARAD point. Elliptical nose shapes are not precluded by the data, but the eccentricity is indeterminate given only one data point on the nose. Figure 5 shows the reconstructed final ablated shape. The total recession is 4.45 ± 0.25 cm at the nose, decreasing to a minimum of 2.74 ± 0.15 cm at midfrustum, then increasing markedly to 4.00 ± 0.15 cm at the frustum near the

Table 3 Curve-fit parameters ($\Delta t = 0.5$ s)

ARAD	i	c_i, s^{-1}	t_{mi}, s	s_{mi}, cm	Δs_i, cm
1, 2	1	0.18	51.0	4.13	0.25
3	2	0.18	51.0	2.77	0.25
4	3	0.19	50.5	2.74	0.15
5, 6	4	0.19	49.5	3.13	0.15
7, 8	5	0.19	49.0	3.63	0.15
9, 10	6	0.19	51.5	2.58	0.15

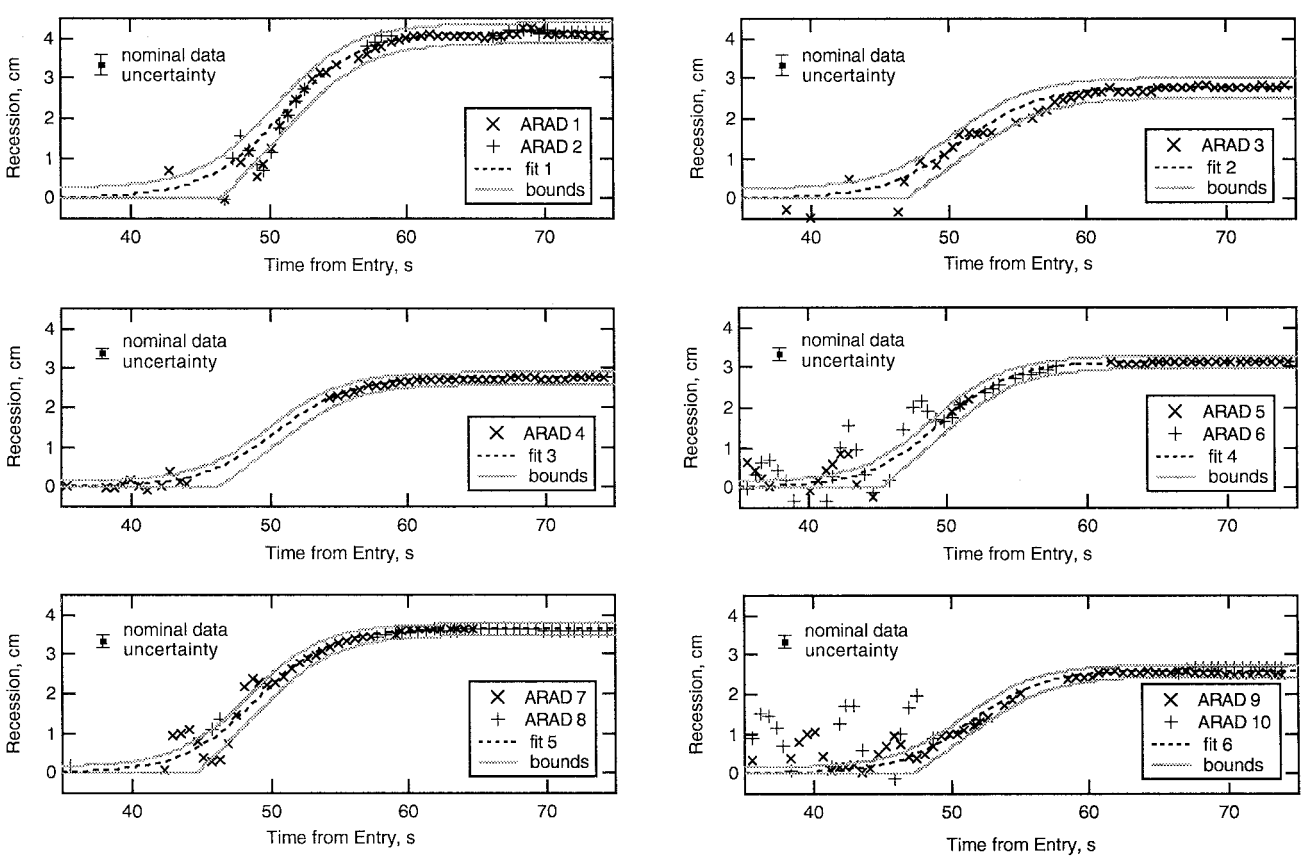

Fig. 4 ARAD recessions and curve fits, sorted by S/R_N location.

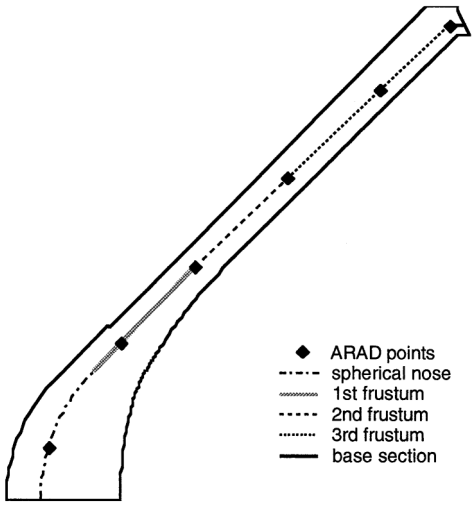

Fig. 5 Reconstruction of heatshield final shape (to scale with initial centerline thickness of 14.6 cm).

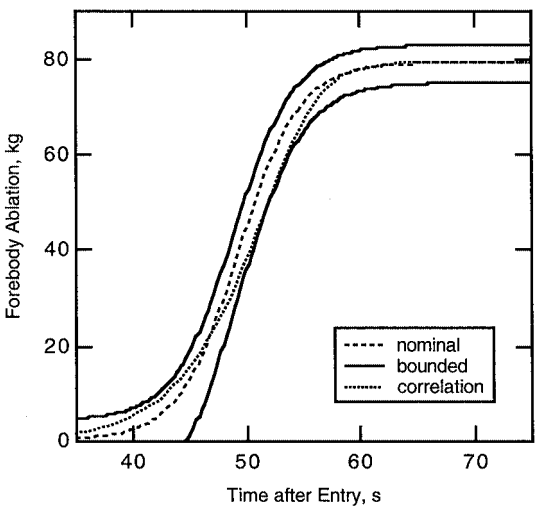

Fig. 6 Forebody ablative mass loss history.

base. More than 10 cm of heatshield remained unablated at the nose, but only 1.40 ± 0.15 cm was not ablated at the end of the frustum. The most critical location is the small base section at the back of the frustum heatshield (cf. Fig. 1) where the data from ARADs 9 and 10 indicate the final heatshield thickness was 1.08 ± 0.15 cm.

The forebody ablative mass loss (Fig. 6) is calculated analytically from the shape histories obtained using the fitting and bounding functions. The bounding curves in Fig. 6 differ by almost 18 kg at 45.25 s, but this difference decreases to 8 kg in the postablation regime. The nominal shape history produces a relatively symmetrical curve with a maximum ablation rate of 7.4 kg/s at 49.7 s. Consistent with preflight predictions,[2,19,20] 90% of the ablation occurs in about 16 s. Figure 6 also shows an empirical mass loss correlation,[21] $dM/dt = K\rho_\infty V_\infty^{6.9}$, derived from strongly radiating viscous shock layer solutions,[2] where the constant K was adjusted to match the nominal mass loss of 79 kg. The correlation predicts a greater mass loss than the nominal curve at early time, but a lower maximum ablation rate of 6.2 kg/s at 51.6 s. Although the preflight predictions did not reproduce the recession distribution accurately; nevertheless, the correlation lies within the uncertainty defined by the bounding curves.

The qualitative agreement of the correlation with the curve fits provides a validation of the recession data timing used in this work. Reference 7 suggests that the ARAD data and curve fits should be shifted 6.25 s later in time. This alternative timing would shift the nominal and bounded curves 6.25 s to the right in Fig. 6. Although not physically impossible, this alternative timing seems unlikely because the nominal and bounded curves would all lie to the right of the correlation, and almost 40% of the mass loss would occur after peak deceleration (which occurs at 57.2 s).

Temperature Sensors and Data

Four resistance thermometers, T_1–T_4, were bonded to the inside of the structure at the locations[14] shown in Fig. 2. T_1 was located inside the nosecap, T_2 was inside the frustum at approximately the same S/R_N of ARADs 7 and 8, T_3 was off the aft centerline, and T_4 was near the edge of the aft cover. As shown in Fig. 7, the thermometer body was aluminum with a flat octagonal shape 3.18 cm across and 0.318 cm thick.[22] The thermometers were bonded to the structure with Eccobond 57C, a high-density electrically conductive epoxy.[10] Materials and thicknesses at the four thermometer locations are given in Table 4.[3,10,23–26] The Eccobond thickness, which was not specified, is assumed to be 0.0254 cm.

The thermocouple body contained a small nickel element with an electrical resistance that varied approximately linearly with temperature from 250 to 450 K. The precise variation of each sensor was recorded as an 11-point calibration curve over this temperature range.[15] During probe entry, the sensor voltage at fixed current was recorded as a count value, which is easily converted to temperature by interpolation of the known calibration curve. Data from each thermometer were recorded every 8 s, and six samples from each thermometer were stored in recycling memory.[14] Temperature data acquisition was intended to stop immediately after termination of recession data acquisition, but the stop command was never issued because of unintended command sequences caused by the acceleration switch cross wiring in the probe.[7] Thus, temperature data continued to be taken and overwritten in memory for another 109.7 s until data acquisition was interrupted by the parachute-deployment sequence (which also occurred about 53 s late because of the unintended command sequences).[7]

The temperature data[7] are presented in Fig. 8 and in Table 5. Nosecap thermometer T_1 showed no response, which was expected

Table 4 Materials and thicknesses

Element	Material	Thickness
Heatshield	Carbon phenolic	14.5 cm (T_1), 5.30 cm (T_2)
Bond	EA 934	0.1524 ± 0.0508 cm
Structure	Al 7075	0.0762 cm
Heatshield	Phenolic nylon	1.04 cm (T_3), 0.89 cm (T_4)
Bond	RTV 630	0.1016 ± 0.0508 cm
Structure	Al 6061	0.0762 cm
Bond	Eccobond 57C	0.0254 cm (est.)
Thermometer	Al 6061	0.3175 cm

Table 5 Temperature data

	Temperature, K			
Time from entry, s	T_1	T_2	T_3	T_4
122.7	260.6	291.1	280.9	284.5
130.7	260.6	299.6	280.9	287.8
138.7	260.6	306.3	283.5	291.0
146.7	263.3	312.9	286.2	292.6
154.7	263.3	319.5	288.8	295.9
162.7	260.6	324.4	288.9	299.1
MST data:	263.3	272.2	275.6	274.8
Minimum uncertainty:	±2.7	±1.7	±2.7	±1.7

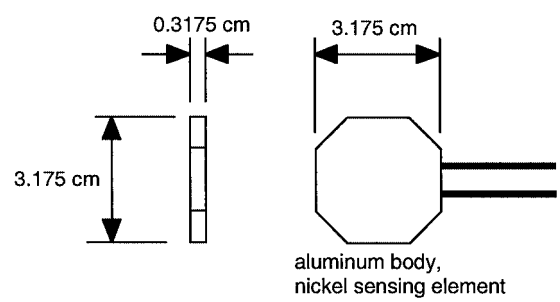

Fig. 7 Resistance thermometer.

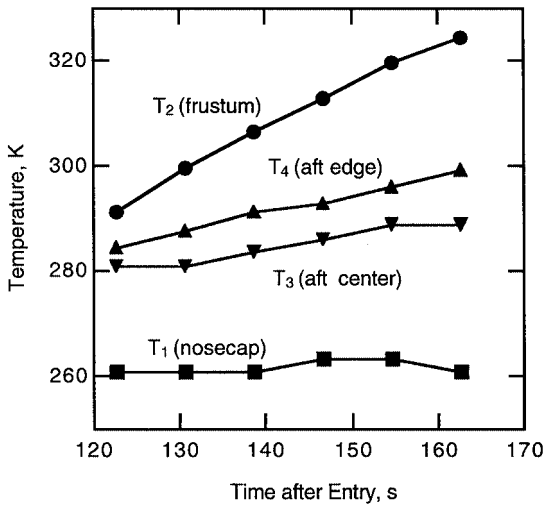

Fig. 8 Temperature data from Galileo resistance thermometers.

because the aerothermal heat pulse could not penetrate through the thickest portion of the heatshield in 160 s. Frustum thermometer T_2 showed a significant response, increasing about 0.83 K/s over the 40-s data window. The aft thermometers T_3 and T_4 recorded minimal temperature increases of about 0.20 and 0.37 K/s, respectively. There is no evidence of sensor drift or data handling errors; therefore, temperature uncertainty is assumed to be ± 1 count, which equals ± 1.7 K or ± 2.7 K as indicated in Table 5. The thermometers and wiring undoubtedly stayed firmly attached to the structure, because otherwise circuit failure would have occured during the severe deceleration of the probe.

The delay in termination of temperature data acquisition was fortuitous in the sense that no temperature rise would have been observed if data acquisition had terminated as intended (109.7 s earlier). One disadvantage of the delay, however, is the lack of an initial condition for the experiment, i.e., the pre-entry temperatures were not saved. The only useful reference data are from the 1992 mission sequence test (MST),[17] which recorded the temperatures also listed in Table 5. These temperatures are consistent with preflight vacuum-test data, which showed the interior structure temperatures varying from 261 K inside the nose to 277 K inside the aft cover.[3] The vehicle was wrapped with multilayer insulation and thermal control blankets except at the nose, which was intended to be the coldest spot at entry. By design, at the locations of thermometers T_2–T_4 prior to entry the temperature should remain near 273 K, and there should only be a small temperature gradient across the heatshield material at these locations due to the surface insulation. It is possible some insulation may have been lost or loosened at separation of the deceleration module from the orbiter in July 1995, but there was no indication of lower temperatures inside the probe that would have resulted from space exposure of additional heatshield surface area.

Thermal Models and Analysis

One-dimensional transient analyses of heatshield ablation, pyrolysis, and heat conduction were performed using the FIAT code developed at NASA Ames Research Center.[27] Multidimensional axisymmetric heat conduction analyses were performed using COSMOS/M finite element software,[28] because simulation of the thermometer temperatures was found to be a multidimensional heat conduction problem. The finite element model contained only the innermost portion of the heatshield that did not char, the attached structure, and the thermometer. The boundary condition for the finite element analysis was a temperature history obtained from the FIAT code. The primary purposes of these analyses are to estimate the surface heating that produced the measured temperature or recession response, to determine the consistency of the recession and temperature data, and to compare the results with preflight estimates.

It was unnecessary and beyond the scope of this work to perform fluid dynamic calculations to predict heatshield convective and radiative heating histories. Instead, a net surface heat flux was prescribed as a simple triangular function, shown in Fig. 9, and the computational surface energy balance was modified to eliminate convective heating and blowing reduction terms.

Table 6 Carbon phenolic properties

T, K	c_p, J/kg-K	k_v, W/m-K[a]
255.6	796	0.623
422.2	1323	0.760
533.3	1507	0.854
811.1	1674	1.109
1088.9	1842	1.346
1366.7	1925	1.589
1644.4	2051	1.826
1922.2	2135	2.069
2777.8	2386	2.773

[a]Model assumes $k_c = 0.87 k_v$.

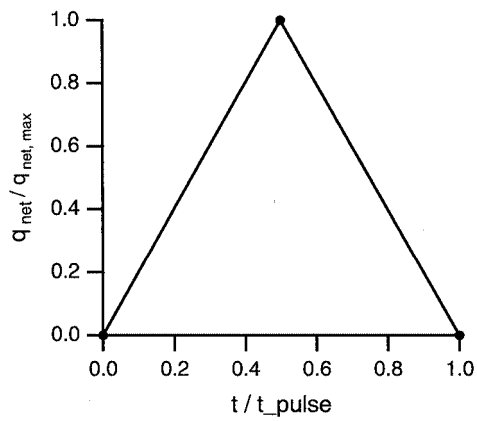

Fig. 9 Triangular heating function for FIAT analyses.

For carbon phenolic, the MAT code[29] was used to generate dimensionless tables for ablation and pyrolysis into a Jovian atmosphere containing helium mass fraction 0.238. The surface energy balance was written as

$$q_{\text{net}} = q_{\text{cond}} + \sigma \varepsilon T_s^4 + (\dot{m}_c + \dot{m}_g) h_w - \dot{m}_c h_c - \dot{m}_g h_g \qquad (2)$$

where the wall-gas enthalpy h_w is a dependent variable in the ablation tables.

For phenolic nylon, the original heatshield design calculations[19] used a simple effective heat of ablation Q^* model to predict the surface recession. A constant value $Q^* = 81.4$ MJ/kg was used in conjunction with a fixed-ablation temperature greater than 1111 K. It is not known exactly how this model was implemented in the design analyses, which used the REKAP code,[30] but in this work the surface energy balance was written as

$$q_{\text{net}} = q_{\text{cond}} + \sigma \varepsilon T_s^4 + \dot{s} \rho_s Q^* \qquad (3)$$

where

$$\dot{s} = 0 \quad \text{if} \quad T_s < T_{\text{abl}}, \qquad T_s = T_{\text{abl}} \quad \text{if} \quad \dot{s} > 0$$

An ablation temperature of 1225 K was found to provide a good reproduction of earlier calculations.

Material properties, given in Tables 6–9, were obtained from the original REKAP input decks and output files, the thermal protection systems expert and material property database (TPSX),[31] and/or the bond manufacturers. The carbon phenolic and phenolic nylon models are similar to those recommended by Bueche[32] and Kottock,[33] respectively. For Table 6 (carbon phenolic properties), the kinetic equation is

$$\frac{\partial \rho}{\partial t} = -A \exp\left(\frac{E}{RT}\right) \rho_v \left(\frac{\rho - \rho_c}{\rho_v}\right)^{\eta} \qquad (4)$$

Table 7 Phenolic nylon properties

T, K	c_p, J/kg-K	k_v, W/m-K[a]
255.6	1193	0.231
311.1	1453	0.231
366.7	1708	0.231
422.2	1823	0.231
477.8	1938	0.231
533.3	1832	0.231
811.1	2081	0.249
1088.9	2135	0.271
1366.6	2311	0.389

[a]Model assumes $k_c = 3.64k_v$

Table 8 RTV bond properties (1394 kg/m^3)

T, K	c_p, J/kg-K	k_v, W/m-K
255.6	1047	0.355
311.1	1193	0.338
366.7	1298	0.319
422.2	1382	0.304
477.8	1465	0.292
533.3	1528	0.280
811.1	1675	0.280

Table 9 Other material properties

Material	ρ, kg/m^3	c_p, J/kg-K	k, W/m-K
EA934	1314	1382	0.33
Eccobond	3500	1089	8.1
Aluminum	2707	879	137

where $\rho_v = 1448$ kg/m^3, $\rho_c = 1185$ kg/m^3, $\eta = 2$, $A = 0.2$ s^{-1} ($T < 720$ K), $A = 11{,}000$ s^{-1} ($T > 720$ K), $E/R = 2600$ K ($T < 720$ K), $E/R = 10{,}736$ K ($T > 720$ K), and $\varepsilon = 0.85$. For Table 7 (phenolic nylon properties), $\rho_v = 1201$ kg/m^3, $\rho_c = 300$ kg/m^3, $A = 4.45e+7$ s^{-1}, $\eta = 3$, $E/R = 15{,}935$ K, $\varepsilon_v = 0.87$, and $\varepsilon_c = 0.65$.

Frustum Heating

Frustum thermometer T_2 was located at the S/R_N location of ablation sensors 7 and 8, where the initial heatshield thickness was 5.3 cm and the measured recession was 3.63 ± 0.15 cm. Nominal and bounded recession histories are given by curve-fit equations and parameters in Table 3. To use the ablation tables, a pressure and an effective mass transfer coefficient must be specified. Preflight calculations showed the frustum surface pressure to be in the range of 1–5 atm over the peak heating portion of the nominal trajectory.[2,3] The mass transfer coefficent is unknown, but values in the range 0.01–0.05 kg/m^2-s were found to provide peak surface temperatures in the desired range[2,20] of 3800–4100 K.

Four calculations were performed using constant values of pressure and mass transfer coefficient equal to the bounds given earlier. In each case the peak heat flux was adjusted to match the nominal recession, and the heat pulse was centered at 49 s to match parameter t_{mi} in Table 3. A good match to the nominal recession history was obtained using a heat pulse duration, a peak heat flux, and an integrated heat load of 24 s, 13.4 kW/cm^2, and 161 kJ/cm^2, respectively. The latter quantities varied by only 1% between the four cases; therefore, for subsequent runs the pressure and effective mass transfer coefficient were taken to be 3 atm and 0.025 kg/m^2-s.

Three solutions (labeled simulation in Fig. 10) were obtained to match the minimum, nominal, and maximum final recession. The bounding peak heat flux and heat load were 13.4 ± 0.5 kW/cm^2 and 161 ± 6 kJ/cm^2. Results from these cases are presented in Figs. 11–13. The surface temperature histories (Fig. 11) show a peak temperature near 4000 K and surface cooling by reradiation following the heat pulse. The bondline and structure temperatures reach 340–381 K at 167 s after entry. These values are safely below the design limits of 644 and 589 K for the bondline and structure, respectively.

Figure 12 shows one-dimensional in-depth temperature histories computed for the nominal recession with and without the thermocouple bonded to the back of the structure. The bondline and structure temperatures are strongly affected by the presence of the thermometer, which has a high conductivity and a significant mass. The presence of the thermometer does not, however, significantly affect the heatshield temperature 1 cm from the bondline (4.3 cm from the original surface) on the time-scale shown in Fig. 12. This latter temperature, therefore, can be used as a boundary condition for a multidimensional heat conduction solution of the structure with an

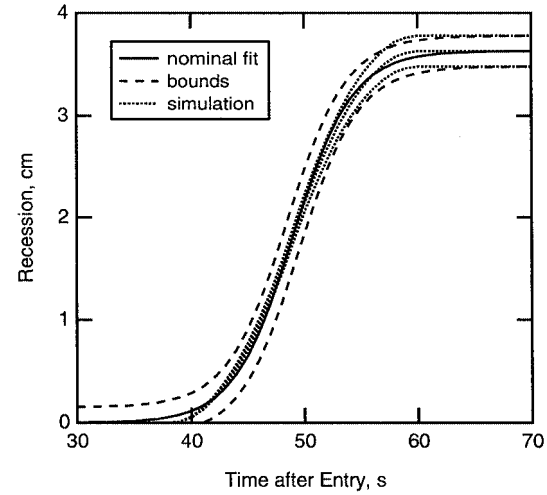

Fig. 10 Surface recession histories.

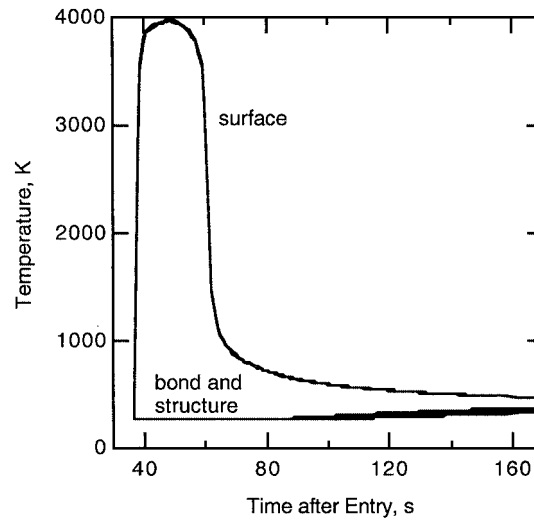

Fig. 11 Temperature histories for frustum nominal case.

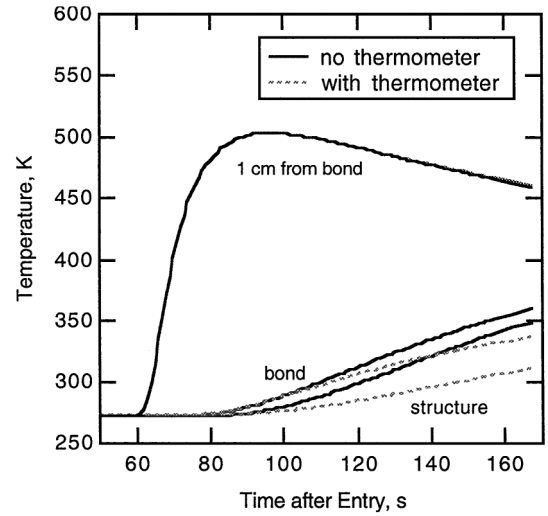

Fig. 12 In-depth temperature histories for nominal case.

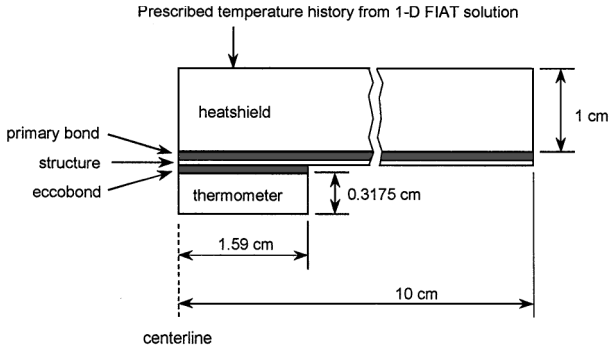

Fig. 13 Axisymmetric model geometry for multidimensional heat conduction solutions.

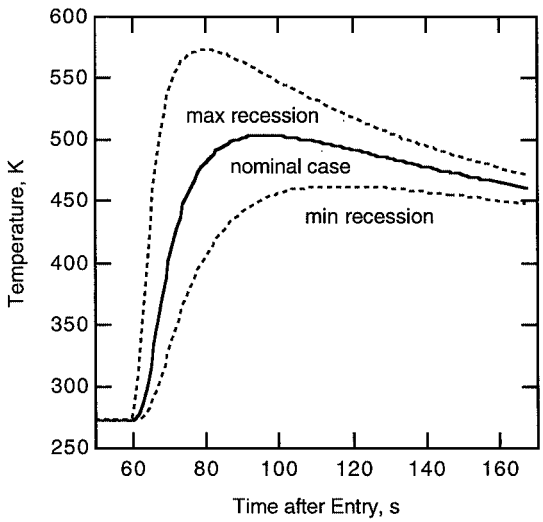

Fig. 14 Temperature histories, at 4.3-cm depth, used as boundary conditions for axisymmetric model.

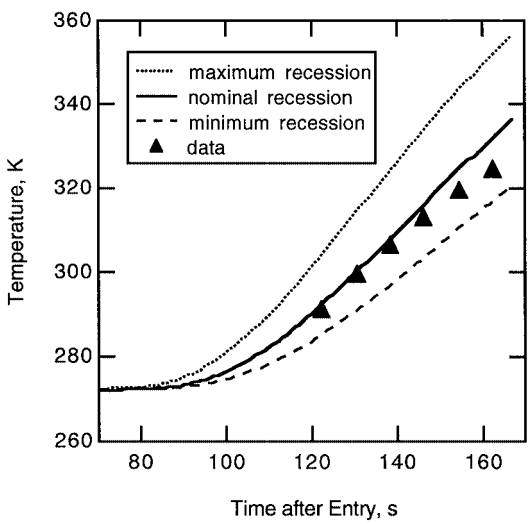

Fig. 15 Data and FIAT predictions for frustum thermometer T_2.

attached thermometer. The axisymmetric model, shown in Fig. 13, included 1 cm of virgin carbon phenolic, and the inner surfaces were assumed to be insulated. The boundary condition temperature histories for the three cases are shown in Fig. 14. The maximum recession case shows a pronounced maximum temperature of 572 K at 80 s, whereas the minimum recession case shows a broad maximum near 460 K between 65 and 100 s.

The temperature at the center of the thermometer for the three cases is compared with T_2 data in Fig. 15. The recession magnitude has a strong influence on the slope of the temperature response, and the agreement between the data and predictions is excellent, with the data falling slightly below the solution for the nominal case. Thus, the temperature and recession data reduction are consistent at this frustum location. The only discrepancy is the data appear to have downward curvature that is not seen in the predictions until a later time than shown in Fig. 15. This downward curvature may indicate a convective cooling (not modeled) of the surface by the low-temperature atmosphere after the end of the primary heat pulse. It should be noted that if the alternative ablation-data timing is used, the three curves are shifted 6.25 s to the right in Fig. 15; then the temperature data lie between the maximum and nominal curves. Because either timing provides self-consistent results, the temperature data do not resolve the uncertainty in ablation data timing.

Aft Heating

The Galileo probe aft heatshield design calculations used an effective heat of ablation model for phenolic nylon. Although input decks were found, full details of the original model are unknown because that option is no longer implemented in the REKAP code. For the present work, an ablation temperature was determined by comparing FIAT solutions with the REKAP solution from Ref. 19. In that reference, for a lighter (290-kg) probe, the design thickness at the aft centerline was 0.472 cm of phenolic nylon, 0.102 cm of DC 93-500 silicone bond, and 0.165 cm of aluminum structure. A cumulative heat flux of about 15 kJ/cm^2 produced recession of 0.37 cm and a maximum bondline temperature of 644 K, which is the design limit. FIAT solutions were obtained using the stagnation-point heating rate from Ref. 19 and material properties from the REKAP input decks. Scaled RTV properties were used for the bond, because DC 93-500 properties were not available. A good match to the REKAP solution was obtained using an ablation temperature of 1225 K, which resulted in 0.35 cm of recession. The REKAP and FIAT temperature predictions are compared in Fig. 16. The good agreement between the temperature predictions and the approximate match of total recession suggests that FIAT is adequately reproducing the phenolic nylon material model used in the design calculations.

For the aft heatshield of the Galileo probe, the final design predictions for a nominal entry and atmosphere used heat loads of 16–20 kJ/cm^2, which were predicted to cause 0.41–0.51 cm of recession.[3] Addition of 0.24 cm of material for insulation of the bondline and a 50% margin for recession resulted in a final design thickness of 0.89–1.04 cm for the aft cover.[3] Thermometer T_3 was located between the centerline and the middome position, and thermometer T_4 was located near the outer dome location at the edge of the aft cover (cf. Fig. 2). For a nominal entry the predicted heat load at both locations[3] was about 17.3 kJ/cm^2, but the heatshield was 0.15 cm thinner at the location of T_4.

Unlike the frustum calculations discussed earlier, where the measured recession provided constraints for the timing and magnitude

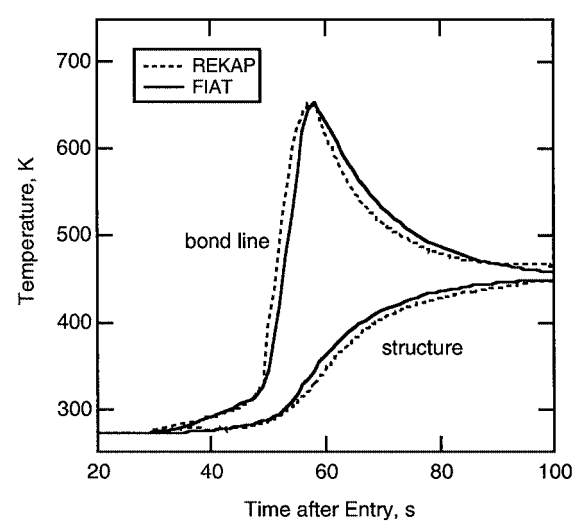

Fig. 16 FIAT and REKAP predictions for in-depth temperature histories at aft centerline (290-kg probe).

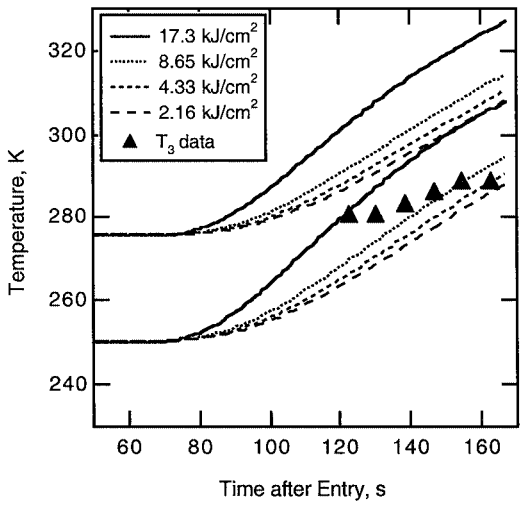

Fig. 17 Data and FIAT predictions for aft thermometer T_3.

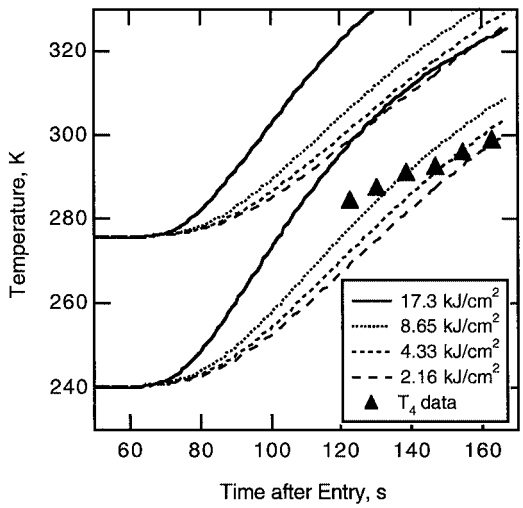

Fig. 18 Data and FIAT predictions for aft thermometer T_4.

of the surface heating, for the aft calculations no surface data or constraints are available. Therefore, lacking such additional data, the same triangular heating pulse and timing were used for both frustum and aft heatshield calculations. FIAT solutions were obtained using heat loads of 17.3, 8.65, 4.33, and 2.16 kJ/cm^2 applied over 24 s and using the estimated initial temperatures given in Table 5. The runs were then repeated using a lower initial temperature of 240 K. A low initial temperature is possible if the aft blanket detached from the heatshield prior to entry, but there is no indication that such an event happened.

The FIAT solutions provided temperature histories, at a location 0.508 cm from the original heatshield surface, which were input as boundary conditions for an axisymmetric finite element calculation of the thermometer temperature history. The distance of 0.508 cm was selected to ensure phenolic nylon charring did not occur within the domain of the finite element model. Thermometer temperature predictions are compared with the data for T_3 and T_4 in Figs. 17 and 18, respectively. For cases that used the in-flight temperatures as an initial condition, it is obvious that no case provides a good match to either the magnitude or the slope of the temperature data. The cases with a low initial temperature envelop the data, but the predicted slopes are too high. The low slope of the temperature data is difficult to explain because once the material conducts energy inward from the surface, the heat pulse inexorably must penetrate to the thermometer regardless of subsequent surface cooling that may occur. The data seem to indicate an unexpected low heat conduction into the aft heatshield. Whether this discrepancy should be attributed to excessively high heating estimates, deficiencies of the material modeling, or other factors is unknown at this time.

Conclusions

The Galileo Probe deceleration module contained instrumentation to measure heat shield ablation and temperatures during the hypersonic entry into the Jovian atmosphere. The experimental setup and data acquisition were described, and the reduced data were presented. One-dimensional transient analyses of the heatshield ablation, pyrolysis, and heat conduction were performed at the thermometer locations. These calculations were coupled with an axisymmetric heat conduction model to predict the thermometer temperature response. Near the end of the frustum, the temperature and recession data are very consistent. The measured recession was 3.63 ± 0.15 cm, and the estimated peak heat flux and heat load are 13.4 ± 0.5 kW/cm^2 and 161 ± 6 kJ/cm^2, respectively. At the aft cover, results of the material response analyses do not match the low magnitude and slope of the temperature data. The data seem to indicate the heat conduction into the heatshield was unexpectedly low.

Acknowledgments

This work was partially supported by NASA Contract NAS2-14031 to ELORET. The authors thank D. E. Carlock and C. K. Sobeck for their assistance in obtaining reference information, locating design drawings, and processing of the raw experimental data. The forebody ablative mass loss correlation was developed by R. C. Blanchard and A. Seiff.

References

[1]"Galileo Probe System Critical Design Review, Book 1," Hughes Space and Communications Group, Rept. HS373-2275, Hughes Aircraft Co., Nov. 1981.

[2]Moss, J. N., and Simmonds, A. L., "Galileo Probe Forebody Flowfield Predictions," *Entry Vehicle Heating and Thermal Protection Systems: Space Shuttle, Solar Starprobe, Jupiter Galileo Probe*, edited by P. E. Bauer and H. E. Collicott, Vol. 85, Progress in Astronautics and Aeronautics, AIAA, New York, 1983, pp. 419-445.

[3]Talley, R. N., "Galileo Probe Deceleration Module Final Report," Re-Entry Systems Operations, Rept. 84SDS2020, General Electric Co., Philadelphia, PA, Jan. 1984.

[4]"Galileo Probe Final Project Report," Space and Communications Group, Rept. HS373-4500, Hughes Aircraft Co., Oct. 1990.

[5]"Heatshield—Nose," Re-Entry Systems Operations, Contract 08-737444-LD4, Drawing 47E526563, General Electric Co., Philadelphia, PA, Aug. 1981.

[6]"Frustum Heatshield," Re-Entry Systems Operations, Contract 08-737444-LD4, Drawing 47E523221, General Electric Co., Philadelphia, PA, Aug. 1981.

[7]"Galileo Probe Mission Operations Final Report," Hughes Space and Communications Co., Rept. HS373-6000, Sept. 1996.

[8]Von Zahn, U., and Hunten, D. M., "The Helium Mass Fraction in Jupiter's Atmosphere," *Science*, Vol. 272, May 1996, pp. 849–851.

[9]Niemann, H. B., Atreya, S. K., Carignan, G. R., Donahue, T. M., Haberman, J. A., Harpold, D. N., Hartle, R. E., Hunten, D. M., Kasprzak, W. T., Mahaffy, P. R., Owen, T. C., Spencer, N. W., and Way, S. H., "The Galileo Probe Mass Spectrometer: Composition of Jupiter's Atmosphere," *Science*, Vol. 272, May 1996, pp. 846–849.

[10]Milos, F. S., "Galileo Probe Heatshield Ablation Experiment," *Journal of Spacecraft and Rockets*, Vol. 34, No. 6, 1997, pp. 705–713.

[11]"Sensor Installation—Aeroshell," Re-Entry Systems Operations, Contract 08-737444-LD4, Drawing 47R523255, rev. C, General Electric Co., Philadelphia, PA, April 1982.

[12]"Analog Resistance Ablation Detector (ARAD)," Re-Entry Systems Operations, Contract 08-737444-LD4, Drawing 47D523037, rev. B, General Electric Co., Philadelphia, PA, Aug. 1979.

[13]"ARAD/HILOK Drilling," Re-Entry Systems Operations, Contract 08-737444-LD4, Drawing SK-777, rev. 5, General Electric Co., Philadelphia, PA, Jan. 1982.

[14]"Galileo Probe Operations Manual," Hughes Space and Communications Group, Rept. HS373-3726A, Hughes Aircraft Co., Nov. 1989.

[15]"Galileo Probe Telemetry Calibration Handbook," Hughes Space and Communications Group, Rept. SS32220-021, rev. A, Hughes Aircraft Co., Jan. 1986.

[16]"Calculation of Delay in Parachute Deployment Attributable to G-Switch Anomaly," Hughes Space and Communications Co., Rept. HS 373-0020-3849, March 1996.

[17]"December 1992 Mission Sequence Test Report," Hughes Space and Communications Co., Rept. HS373-0020-3664, April 1993.

[18]Seiff, A., and Knight, T. C. D., "The Galileo Probe Atmosphere Structure Instrument," *Space Science Reviews*, Vol. 60, No. 1, 1992, pp. 203–232.

[19]Brewer, R. A., and Brant, D. N., "Thermal Protection System for the Galileo Mission Atmospheric Entry Probe," *Aerothermodynamics and Planetary Entry*, edited by A. L. Crosbie, Vol. 77, Progress in Astronautics and Aeronautics, AIAA, New York, 1981, pp. 309–334.

[20]Green, M. J., and Davy, W. C., "Galileo Probe Forebody Thermal Protection," AIAA Paper 81-1073, June 1981.

[21]Seiff, A., Venkatapathy, E., Haas, B. L., and Inteiri, P., "Galileo Probe Aerodynamics," AIAA Paper 96-2451, June 1996.

[22]"Sensor—Temperature," Re-Entry Systems Operations, Contract 08-737444-LD4, Drawing 47R523230, rev. B, General Electric Co., Philadelphia, PA, Dec. 1981.

[23]"Skin, Frustum—Aeroshell," Re-Entry Systems Operations, Contract 08-737444-LD4, Drawing 47R523085, rev. K, General Electric Co., Philadelphia, PA, Oct. 1981.

[24]"Shield and Structure—Aeroshell," Re-Entry Systems Operations, Contract 08-737444-LD4, Drawing 47R523163, rev. AH, General Electric Co., Philadelphia, PA, Feb. 1982.

[25]"Shell—Aft Cover," Re-Entry Systems Operations, Contract 08-737444-LD4, Drawing 47R523081, rev. C, General Electric Co., Philadelphia, PA, July 1979.

[26]"Shield and Structure Assembly—Aft Cover," Re-Entry Systems Operations, Contract 08-737444-LD4, Drawing 47R523157, rev. J, General Electric Co., Philadelphia, PA, Aug. 1981.

[27]Chen, Y.-K., and Milos, F. S., "Ablation and Thermal Response Program for Spacecraft Heatshield Analysis," *Journal of Spacecraft and Rockets*, Vol. 36, No. 3, 1999, pp. 475–483; also AIAA Paper 98-0273, Jan. 1998.

[28]Lashkari, M., "COSMOS/M User Guide, Volume 1," Structural Research and Analysis Corp., Santa Monica, CA, April 1992.

[29]Milos, F. S., and Chen, Y.-K., "Comprehensive Model for Multicomponent Ablation Thermochemistry," AIAA Paper 97-0141, Jan. 1997.

[30]Gordon, P., "Analysis of One-Dimensional Heat Conduction Computer Program," Re-Entry Systems Operations, Rept. GE-RSD TIS-R66S-D10, General Electric Co., Philadelphia, PA, March 1966.

[31]Squire, T. H., Milos, F. S., Hartlieb, G. C., and Rasky, D. J., "TPSX: Thermal Protection Systems Expert and Material Property Database," *ICCE/4, Fourth International Conference on Composites Engineering*, edited by D. Hui, International Community for Composites Engineering and College of Engineering, Univ. of New Orleans, New Orleans, LA, 1997, pp. 937, 938.

[32]Bueche, J. F., "Effects of Improvements and Uncertainties in Thermophysical Properties on Carbon Phenolic Heatshield Thermal Performance Predictions," AIAA Paper 77-787, June 1977.

[33]Kottock, S., "The Development of a Phenolic Nylon Model for a Reaction Kinetics Ablation Program," Re-Entry Systems Operations, Rept. GE-RSD TIS-655D-320, General Electric Co., Philadelphia, PA, Sept. 1965.

R. D. Braun
Guest Editor